Earth-Science Reviews 113 (2012) 161–175

Contents lists available at SciVerse ScienceDirect

Earth-Science Reviews

journal homepage: www.elsevier.com/locate/earscirev

Singular vectors in atmospheric sciences: A review

Emilia Paula Diaconescu *, René Laprise

Centre ESCER (Étude et Simulation du Climat à l'Échelle Régionale), Dept. Earth and Atmospheric Sciences, University of Québec at Montréal, Montréal (Québec), Canada

ARTICLE INFO

Article history:
Received 7 November 2011
Accepted 21 May 2012
Available online 30 May 2012

Keywords:
Singular vectors
Growth rate
Tangent linear model

ABSTRACT

During the last decade, singular vectors (SVs) have received a lot of attention in the research and operational communities especially due to their use in ensemble forecasting and targeting of observations. SVs represent the orthogonal set of perturbations that, according to linear theory, will grow fastest over a finite-time interval with respect to a specific metric. Hence, the study of SVs gives information about the dynamics and structure of rapidly growing and finite-time instabilities representing an important step toward a better understanding of perturbations evolution in the atmosphere. This paper reviews the SV formulation and gives a brief overview of their recent applications in atmospheric sciences. A particular attention is accorded to the SV sensitivity to different parameters such as optimization time interval, norm, horizontal resolution and tangent linear model, various choices leading to different initial structures and evolutions.

Contents

1. Introduction

This review article is aimed at scientists such as climatologists who, while not being experts in Numerical Weather Prediction (NWP), would like to gain some understanding in singular vector (SV) use. The number of studies implying the use of SVs has increased considerably over the last decade. To give a focus and to keep the article to moderate length, we concentrate in particular on the SV formulation and properties.

SVs can be defined in terms of the singular value decomposition of an operator (the so-called forward tangent linear operator) and can be physically interpreted as a set of fastest growing perturbations. The concept of SVs was first introduced by Lorenz (1965) in his analysis of forecast error growth in dynamical systems and developed later by Lacarra and Talagrand (1988). The optimization problem consists in finding the perturbations from a time-evolving model-generated basic state that have maximum growth (or amplification) in a finite interval of time. The solution can be reduced to a singular value decomposition

* Corresponding author at: Department of Earth and Atmospheric Sciences, Université du Québec à Montréal (UQAM), P.O. Box 8888, Stn. Downtown, Montréal (Québec), Canada H3C 3P8. Tel.: +1 514 987 3000x7631.
E-mail address: diacones@sca.uqam.ca (E.P. Diaconescu).

0012-8252 © 2012 Elsevier B.V. Open access under CC BY-NC-ND license.
doi:10.1016/j.earscirev.2012.05.005

of a suitable operator and the resulting SVs provide an orthogonal set of optimal perturbations. They represent the orthogonal set of perturbations that, according to linear theory, will have the maximum growth over a finite-time interval with respect to a specific metric.

The growth of perturbations has been initially studied in simple models with idealized time-independent basic states assuming that the solution of the linear perturbation equations can be expressed as a superposition of orthogonal functions, i.e. normal modes with fixed structure and amplitude varying exponentially with time. However, Farrell (1982, 1985) while studying the growth of perturbations in quasi-geostophic models, found that it is also possible to identify perturbations with growth exceeding, for a limited time, those typical of the fastest growing normal mode. These perturbations have a three-dimensional structure that changes in time, and they were named "non modal perturbations" to distinguish them from the former ones, which have fixed structure during their time evolution and amplitude changing exponentially with time (Montani and Thorpe, 2002). Those studies used stationary basic states. SVs are «finite-time instabilities» (Molteni and Palmer, 1993) that are computed from a time-evolving basic state without assuming a normal-mode solution.

Initially, the SV theory has been applied to a number of idealized studies within the framework of quasi-geostrophic models; it was used for example by Borges and Hartmann (1992) and Molteni and Palmer (1993) in barotropic and baroclinic atmosphere investigations. At the beginning of the 1990s, SV technique began to be computed for primitive-equation models (e.g. the atmospheric general circulation models AGCMs). SVs have since been the subject of numerous studies. They have been used in atmospheric predictability studies (e.g., Palmer et al., 1994; Hakim, 2000; Descamps et al., 2007) and in forecast error estimation (e.g., Ehrendorfer and Tribbia, 1997; Gelaro et al., 1998). In the 90s, SVs began to be used daily to construct the initial perturbations in Ensemble Predictions System (EPS) at the European Centre for Medium-Range Weather Forecasts (ECMWF). Presently they are also used in other forecast centers as Japan Meteorological Agency, Météo-France and Bureau of Meteorology (BoM) in Australia. Because SVs capture the dynamically most unstable perturbations, they identify the directions of initial uncertainty that are responsible for the largest forecast uncertainty. This property made them a very good candidate in producing an ensemble with sufficient dispersion in the most unstable directions (Leutbecher and Palmer, 2008) providing optimal information about the probability density function of the model state at a future time.

Recently, they have been employed to perturb the initial conditions in coupled ocean–atmosphere models of El Niño–Southern Oscillation (ENSO) (Kleeman et al., 2003). Another recent use of SVs is to detect "sensitive" parts of the atmosphere for targeting adaptive observations (e.g. Palmer et al., 1998; Buizza and Montani, 1999; Langland, 2005; Buizza et al., 2007b); by identifying the regions with a large sensitivity to small perturbations they point to where additional observations have the potential to significantly improve weather forecasts (Kim and Jung, 2009a).

The purpose of this paper is to provide an overview of the SV technique. We first review the mathematical formulation of SVs in Section 2 and present the choice of norm in Section 3. The linearization process around a time-evolving model-generated basic state leads to the tangent linear model (TLM). Linearized models have been developed first for the adiabatic part of the forecast model using a simplified scheme for the vertical diffusion. As a consequence, SVs have been obtained initially for dry models (e.g., Buizza et al., 1993; Buizza and Palmer, 1995; Ehrendorfer and Errico, 1995). However, the process of error growth in the atmosphere depends not only on dry dynamics but also on moist diabatic processes such as condensation, evaporation, and moist convection. The reasons for not including moist processes in earlier studies are due to the difficulties involved in finding suitable linear descriptions of moist processes (Errico and Raeder, 1999) especially because the parameterizations of subgrid-scale physical processes introduce "thresholds" that make the model discontinuous. The characteristics of "dry" and "moist" SVs are presented in Section 4, followed by a discussion regarding the SV dependence on the horizontal resolution and optimization time interval. Section 5 gives some examples of SV applications in atmospheric sciences. The paper concludes with a brief discussion of the main results that were presented in the review.

2. Mathematical development of the singular vectors

The mathematical development of SVs has been described in detail first by Lacarra and Talagrand (1988) and later by Buizza et al. (1993) and Kalnay (2003, chap. 6.3). An equivalent mathematical development is presented also by Palmer et al. (1998) using index-based tensor formalism instead of the more conventional matrix notation. In this section, we review the theoretical bases and concepts using the matrix notation.

Consider a non-linear model ($\mathbf{M}$) describing the atmospheric system. The variables needed to represent the atmospheric state of the model, such as temperature, wind and surface pressure, are collected as a column matrix called the state vector $\mathbf{X}$. The time evolution of the state vector $\mathbf{X}$ (i.e. the model tendency equation) can be written in the symbolic form:

$$\frac{d\mathbf{X}}{dt} = \mathbf{F}(\mathbf{X}), \mathbf{X} = \begin{bmatrix} \mathbf{X}_1 \\ \bullet \\ \bullet \\ \bullet \\ \mathbf{X}_n \end{bmatrix}, \mathbf{F} = \begin{bmatrix} \mathbf{F}_1 \\ \bullet \\ \bullet \\ \bullet \\ \mathbf{F}_n \end{bmatrix} \tag{1}$$

were $\mathbf{X} \in \mathrm{R}^{\mathrm{N}}$ denotes the N-dimensional state vector and $\mathbf{F}(\mathbf{X}) \in \mathrm{R}^{\mathrm{N}}$ its tendency which includes the dynamical and the physical parameterization contributions.

Let $\mathbf{X}(\mathrm{t})$ be a solution of Eq. (1). Finding the solution consists in generating a trajectory from an initial point $\mathbf{X}(\mathrm{t}_0)$ to $\mathbf{X}(\mathrm{t})$ or to integrate Eq. (1) from t_0 to t. This is equivalent to looking at the model (the non-linear propagator $\mathbf{M}$) as a mapping of the initial-time vector $\mathbf{X}(\mathrm{t}_0)$ onto a vector of predictions $\mathbf{X}(\mathrm{t})$:

$$\begin{array}{l} \mathbf{M}: \mathbf{R}^n \rightarrow \mathbf{R}^n \\ \mathbf{X}(t_0) \rightarrow \mathbf{X}(t) \end{array} \tag{2}$$

$$\mathbf{X}(t) = \mathbf{M}(\mathbf{X}(t_0)). \tag{3}$$

The process of finding the optimal perturbations for a given basic state starts with the linearization of the non-linear model around the basic state, defined as the solution of the non-linear model or the trajectory in the space of states. Let $\boldsymbol{x}(t)$ be a small perturbation from the non-linear model trajectory $\mathbf{X}(\mathrm{t})$. Eq. (1) can be written using the first-order Taylor–Young formula in the vicinity of the basic state $\mathbf{X}(\mathrm{t})$:

$$\frac{d}{dt}(\mathbf{X}(t)+x(t)) = \mathbf{F}(\mathbf{X}(t)+x(t)) = \mathbf{F}(\mathbf{X}(t)) + \left.\frac{\partial \mathbf{F}}{\partial \mathbf{X}}\right|_{\mathbf{X}(t)} x(t) + O\left(x^2(t)\right) \tag{4}$$

For short time internals and small perturbations, the terms $O(x^2(t))$ can be neglected, and, after the subtraction of Eq. (1) from Eq. (4), the equation becomes

$$\frac{dx}{dt} = \left.\frac{\partial \mathbf{F}}{\partial \mathbf{X}}\right|_{\mathbf{X}(t)} x = \mathbf{A}_{\mathbf{F}} x \tag{5}$$

were $\mathbf{A}_{\mathbf{F}}$ is the Jacobian of $\mathbf{F}$: $(\mathbf{A}_{\mathbf{F}})_{jk} = \dfrac{\partial \mathbf{F}_j}{\partial \mathbf{X}_k}$. Eq. (5) defines the tangent linear model (TLM) equation. Its integration gives the evolved

perturbation $\boldsymbol{x}(t)$ from any initial perturbation $\boldsymbol{x}(t_0)$ via an integration of the tangent linear model:

$$x(t) = \mathbf{L}(t_0, t)x(t_0) \tag{6}$$

Therefore, the operator $\mathbf{L}(t_0,t)$ that is named the forward tangent linear, or the linear propagator, can be regarded as a mapping of the initial-time perturbation $\boldsymbol{x}(t_0)$ onto the evolved perturbation $\boldsymbol{x}(t)$. Eq. (6) can be obtained equivalently by linearizing Eq. (3):

$$x(t) = \left.\frac{\partial \mathbf{M}}{\partial \mathbf{X}}\right|_{\mathbf{X}(t)} x(t_0) = \mathbf{L}(t_0, t)x(t_0) \tag{7}$$

Because $\mathbf{L}(t_0, t) = \left.\frac{\partial \mathbf{M}}{\partial \mathbf{X}}\right|_{\mathbf{X}(t)}$ it is also named the differential or first derivative of $\mathbf{M}$ (the non-linear model) at point $\mathbf{X}(t)$. The equation shows that $\mathbf{L}(t_0,t)$ depends on the non-linear trajectory $\mathbf{X}(t)$, which evolves in time, but not on the perturbation $\boldsymbol{x}(t)$.

The second step in the optimal perturbation problem is to find those perturbations that have maximized amplitude growth over a finite interval of time. This can be done by finding the SVs of the forward tangent linear $\mathbf{L}$ through a singular value decomposition, which states that every matrix $\mathbf{L}$ can be decomposed as

$$\mathbf{L} = \mathbf{W}\Lambda\mathbf{Y}^*, \tag{8}$$

where Λ is a diagonal matrix with non-negative real numbers on the diagonal. $\mathbf{W} = (\boldsymbol{w_1}, \boldsymbol{w_2}, \ldots, \boldsymbol{w_i}, \ldots, \boldsymbol{w_n})$ and $\mathbf{Y} = (\boldsymbol{y_1}, \boldsymbol{y_2}, \ldots, \boldsymbol{yi}, \ldots, \boldsymbol{y_n})$ are orthonormal matrices and $\mathbf{Y}^*$ denotes the conjugate transpose of $\mathbf{Y}$. The columns of $\mathbf{Y}$ are named the right singular vectors (or the initial SVs) of $\mathbf{L}$, while the columns of $\mathbf{W}$ are named the left singular vectors (or the final SVs) of $\mathbf{L}$. The diagonal elements of Λ, $\mathrm{diag}(\lambda_1, \lambda_2, \ldots, \lambda_i, \ldots, \lambda_n)$, are the singular values and they are ordered so that $\lambda_1 \geq \lambda_2 \geq \ldots \geq \lambda_i \geq \ldots \geq \lambda_n$. The relationship between each «i» initial and final SV is expressed by:

$$\mathbf{L}(t_0, t)y_i = \lambda_i w_i \tag{9}$$

Singular value decomposition and eigenvalue decomposition are closely related because the SVs of matrix $\mathbf{L}$ can be also obtained as the eigenvectors of $\mathbf{L}^*\mathbf{L}$. Generally, the operator $\mathbf{L}$ is not normal ($\mathbf{L}^*\mathbf{L} \neq \mathbf{L}\mathbf{L}^*$). Normal operators ($\mathbf{S}^*\mathbf{S} = \mathbf{S}\mathbf{S}^*$) are important because they can be diagonalized and spectrally decomposed in terms of orthogonal eigenvectors. However, because $\mathbf{L}$ is not generally normal, a traditional empirical orthogonal function (**EOF**) analysis for $\mathbf{L}$ yields eigenvectors that are not orthogonal to one another. Nevertheless, the operator $\mathbf{L}^*\mathbf{L}$ is symmetric and positive definite, and therefore it is a normal operator with mutually orthogonal eigenvectors. The eigenvectors of $\mathbf{L}^*\mathbf{L}$ ($\mathbf{L}\mathbf{L}^*$) are the right (left) SVs of $\mathbf{L}$ and the eigenvalues of $\mathbf{L}^*\mathbf{L}$ (and $\mathbf{L}\mathbf{L}^*$) are the square of the singular values of $\mathbf{L}$:

$$\mathbf{L}^*\mathbf{L}y_i = \lambda_i^2 y_i \tag{10}$$

$$\mathbf{L}\mathbf{L}^* w_i = \lambda_i^2 w_i \tag{11}$$

Consider now the problem of finding the perturbations with maximized amplitude growth over a finite interval of time. Because the space of solutions is a vector space, the magnitude of perturbations will be defined by a norm. In a vector space the norm is a function that maps vectors to their magnitude; in other words it is a function that assigns a strictly positive length to vectors from a space of vectors. We shall refer to $\|\bullet\|_E$ as the $\mathbf{E}$-norm and we shall assume that the solution space is an inner-product space so that the norm can be defined via an inner product,

$$\|x\|_E^2 = \langle x; Ex\rangle = x^T Ex, \tag{12}$$

where $\mathbf{E}$ is a matrix operator that defines the specific form of the inner product. It is important to note that the choice of metric is not unique; but $\mathbf{E}$ defines a valid norm if and only if $\mathbf{E}$ is Hermitian positive definite.

For any linear operator $\mathbf{L}$ on an inner-product space, there is a unique operator $\mathbf{L}^*$, called the adjoint of $\mathbf{L}$ (conjugate transpose of $\mathbf{L}$) with respect to the norm $\mathbf{E}$, such that $\langle x; \mathbf{L}y\rangle = \langle \mathbf{L}^* x; y\rangle$ for all x, y in the space. For systems with real variables, the adjoint and the transpose are identical ($\mathbf{L}^* = \mathbf{L}^{\mathrm{T}}$).

Different norms can be considered at the initial and final times. Consider now a perturbation with the norm at initial time $\mathbf{E_0}$

$$\|x(t_0)\|_{E_0}^2 = \langle x(t_0); E_0 x(t_0)\rangle \tag{13}$$

and at final time with the norm $\mathbf{E_t}$

$$\|x(t)\|_{E_t}^2 = \langle x(t); E_t x(t)\rangle. \tag{14}$$

We are interested in the initial perturbations that maximize the amplification factor in the interval of time (t_0, t), named optimization time interval (OTI). The amplification factor is sometimes named in literature as the growth rate, and it can be measured as the norm at final time divided by the norm at initial time:

$$\lambda^2 = \frac{\|x(t)\|_{E_t}^2}{\|x(t_0)\|_{E_0}^2} \tag{15}$$

Using Eq. (6) and the definition of adjoint operator, the amplification factor can be expressed as

$$\lambda^2 = \frac{\langle \mathbf{L}x(t_0); E_t \mathbf{L}x(t_0)\rangle}{\langle x(t_0); E_0 x(t_0)\rangle} = \frac{\langle \mathbf{L}^* E_t \mathbf{L}x(t_0); x(t_0)\rangle}{\langle x(t_0); E_0 x(t_0)\rangle} \tag{16}$$

Since E_0 and E_t are Hermitian positive definite, they are self-adjoint ($E_0{}^* = E_0$; $E_t{}^* = E_t$). The fastest growing perturbations are obtained by maximizing Eq. (16), and the solution is given by the following generalized eigenvalue problem:

$$(\mathbf{L}^* E_t \mathbf{L})y_i(t_0) = \lambda_i^2 E_0 y_i(t_0), \tag{17}$$

If different norms are used at initial and final times ($E_0 \neq E_t$), the form equivalent to the Eq. (10) is obtained by using the variable transformation, $y_i(t_0) = E_0^{-\frac{1}{2}}\gamma_i(t_0)$:

$$\left(E_0^{-\frac{1}{2}}\mathbf{L}^* E_t \mathbf{L} E_0^{-\frac{1}{2}}\right)\gamma_i(t_0) = \lambda_i^2 \gamma_i(t_0) \tag{18}$$

In Eq. (10), $y_i(t_0)$ are the eigenvectors of $\mathbf{L}^*\mathbf{L}$ and the initial singular vectors of $\mathbf{L}$. By analogy, the eigenvectors of $E_0^{-1/2}\mathbf{L}^* E_t \mathbf{L} E_0^{-1/2} = (E_0^{-1/2}\mathbf{L}E_t^{1/2})^*(E_t^{1/2}\mathbf{L}E_0^{-1/2}) = \mathbf{L}_s{}^*\,\mathbf{L}_s$, are the initial singular vectors of $\mathbf{L}_s = E_t^{1/2}\mathbf{L}E_0^{-\mathbf{1/2}}$, hence, the perturbations with maximized amplification factor in the interval of time (t_0, t). The amplification factors, λ_i^2, are given by the eigenvalues of the generalized eigenvalue problem or by the square of the singular values (λ_i).

The initial SVs form an $\mathbf{E_0}$-orthonormal basis and are ordered according to their amplification factors (λ_i^2) with the fastest growing structure being the first SV. The first SV is also known as the leading SV. Note that the adjoint of $\mathbf{L}(t_0,t)$ is $\mathbf{L}^*(t,t_0)$. The adjoint reverses the direction of time propagation. Therefore the left-hand side of the Eq. (17) involves one integration forward with the TLM, followed by one integration backwards with the adjoint model (ADM). Once the initial-time SVs are obtained, the corresponding final-time SVs (or

evolved SVs) can be computed using $\gamma_i(t) = \mathbf{L}_s\gamma_i(t_0)$ The evolved SVs form an $\mathbf{E_t}$-orthogonal set at optimization time. Note also that SVs are computed following a time-evolving trajectory.

SVs can be computed using the same or different norms at initial and final time. Also, limited-area norms can be used in order to obtain SVs over a geographically restricted region. Hartmann et al. (1995) have used a projection operator that sets the vector to have zero values on grid points outside the region of interest. If a projector operator is used at final time, the SVs are solutions of the following generalized eigenvalue problem:

$$(\mathbf{L}^*\mathbf{P}^*E_t\mathbf{PL})y_i(t_0) = \lambda_i^2 E_0 y_i(t_0) \tag{19}$$

where $\mathbf{P}$ is the projection operator and $\mathbf{P}^*$ is its adjoint. Eq. (19) can be written using the variable transformation, $y_i(t_0) = E_0^{-\frac{1}{2}}\gamma_i(t_0)$, in the form

$$\left(E_0^{-\frac{1}{2}}\mathbf{L}^*\mathbf{P}^*E_t\mathbf{PL}E_0^{-\frac{1}{2}}\right)\gamma_i(t_0) = \lambda_i^2\gamma_i(t_0). \tag{20}$$

The use of the local projector operator $\mathbf{P}$ is relevant especially for the limited-area models and in the particular cases of targeting observations. These SVs are also referred to as "targeted SVs". For complex primitive-equation models, the matrix $\mathbf{L}$ exists only as an operator in the form of a computer code. In this case, the SVs are most easily obtained using an iterative Lanczos algorithm that does not require an explicit representation of the model operator (Buizza et al., 1993; Errico et al., 2001).

Usually SVs are normalized to have unit norms at initial time. Hence, the evolved leading SV will give the direction in the phase space with maximum amplification or growth. Therefore, the first n SVs permit to span the phase space in the n most unstable directions. These directions will define the n-dimensional unstable subspace of the system and they are considered to lead to sufficient forecast spread (Gelaro et al., 1998) and to explain a large part of forecast uncertainty in EPSs. In EPSs, experiments made with different numbers of SVs showed that the ensemble skill increases with increasing the number of SVs. The number of SVs is then decided by the number beyond which the ensemble skill does not improve significantly (Leutbecher and Palmer, 2008). For example, in the ECMWF EPS there are 50 SVs that are computed over the extratropical North Hemisphere and other 50 SVs that are computed over the extratropical South Hemisphere. Another important factor that impose a restriction on the number of SVs is the available computational cost.

Eq. (17) shows that several choices must be made when SVs are computed:

(1) the norms at initial and final time,
(2) the optimization time interval (OTI),
(3) the trajectory,
(4) the TLM and ADM.

Because of the computational cost, usually the TLM and ADM are run at lower resolution and the trajectory comes from a low-resolution non-linear forecast. Several studies have analyzed the SV sensitivity to metric, OTI, TLM, trajectory and resolution (e. g. Buizza, 1998; Palmer et al., 1998; Gilmour et al., 2001; Buehner and Zadra, 2006). In the following, we present a short review of the SV dependence on the choice of norm.

3. Choice of norm

As mentioned above the choice of metric is not unique. One restriction exists: it must be Hermitian positive definite. The most commonly used metrics in the literature are the enstrophy, total energy, kinetic energy and streamfunction variance norm. Palmer et al. (1998) have examined the dependence of SVs on these four norms for one case of middle-latitude SVs in December 1994. They found that at initial time there is a great difference in scales between SVs computed with these four metrics:

(1) the streamfunction norm is characterized by lower to middle troposphere small-scale baroclinic perturbations;
(2) the energy norm produces intermediate-scale baroclinic perturbations;
(3) the enstrophy norm has upper and lower levels large-scale perturbations.

The maxima of either enstrophy or streamfunction SVs do not coincide at initial time with those of the energy SVs. Although the initial-time SVs are quite sensitive to the choice of norm, the final-time SVs are much more similar, presenting a large-scale barotropic aspect. Similar results were obtained by Frederiksen (2000) who has examined the dependence of SVs on the norm during periods of block development, using a two-level model with the upper level at 300 mb and the lower level at 700 mb.

Kalnay (2003, pp. 222–223) interprets the robustness of the SV to the choice of final-time norm as an obvious conclusion from the fact that all perturbations, including SVs, evolve towards the leading Lyapunov Vector that represents the direction in which maximum sustainable long-term growth can occur in a system without external forcing (therefore the system attractor). This idea is also sustained by Trevisan and Pancotti (1998) who have analyzed the Lyapunov Vectors and Singular Vectors in the Lorenz system. Reynolds and Errico (1999) also showed that, into the context of a quasi-geostrophic model, the SVs for optimization times of 5 days or longer converge tower a single pattern, the Lyapunov Vector. They pointed out that the different-metric final-time SV similarity grows very much for very long optimization times (10 to 40 days). The initial-time norm dependence of SVs is explained by Kalnay (2003) by the fact that SVs are initially outside the attractor, pointing to areas in the phase space where solutions do not naturally occur, and they rapidly rotate back into the attractor. The SV transient rapid growth is due to this rapid (one time step) rotation of the initial-time SVs toward the attractor (Szunyogh et al., 1997).

The perturbations as physical structures have to satisfy particular dynamical properties such as “balance conditions”. In their study of the balance of SVs, Montani and Thorpe (2002) pointed out that SVs calculated with enstrophy and kinetic energy norms produce perturbations only with a vorticity component, the temperature part being forced to be zero. They remarked that these kinds of perturbations are by construction unbalanced and therefore, they may produce gravity waves in the first few hours of their time evolution. This means that a certain amount of energy might be radiated away instead of travelling with the perturbations. The fact that the total-energy norm accounts for temperature, wind and surface-pressure disturbances qualifies it as a better candidate for the norm. Montani and Thorpe (2002) showed that the linear balance equation is not satisfied for total-energy perturbations at initial time either, but the SV evolution is such that the unbalanced part observed at initial time is progressively damped with time, so that at optimization time only the balanced part is present. Therefore, the linear balance equation is satisfied at optimization time. This can also be interpreted as the result of the evolution of off-attractor initial-time SVs toward the on-attractor final-time SVs (Szunyogh et al., 1997).

Several studies point out that in EPS and adaptive observations, the most appropriate initial-time norm must be based on the inverse of the analysis-error covariance matrix, (e.g. Ehrendorfer and Tribbia, 1997; Palmer et al., 1998). The argument is that the ICs in NWP are constrained both by the observing network and by the process of assimilating the observations. Buehner and Zadra (2006) compared the analysis-error covariance and the dry total-energy norms for extratropical SVs. They found that the shapes of initial-time SVs are different, but the shape of the evolved SVs is almost independent of the choice of norm. Barkmeijer et al. (1999) tested a norm given by the

Hessian of the cost function of a variational assimilation scheme that is computationally five times more expensive than the total-energy norm. Again, although the Hessian and total-energy SVs present different structures at initial time, there are no significant differences between the results obtained with an ensemble based on Hessian SVs and based on the total-energy SVs. Several authors (e.g., Palmer et al., 1998; Leutbecher, 2007) concluded that among the simple metrics the total-energy metric is a reasonable first-order approximation to an analysis-error covariance metric (Buizza et al., 1997). As a consequence, the most commonly used metric for both initial and final norm even in EPS, is the total-energy norm. However, the correct choice is indeed the analysis-error covariance norm (Ehrendorfer and Tribbia, 1997).

4. Structure and characteristics of SVs

As mentioned in the introduction, the tangent linear models have been developed first for the adiabatic part of a non-linear model because parameterizations of physical processes are highly non-linear and sometimes discontinuous. Also, the inclusion of physical processes in TLM increases the computational cost of SVs considerably (Puri et al., 2001). However, linearized models without physics produce unrealistic results. Buizza (1994) have underlined the necessity of the representation in TLM of vertical diffusion and surface drag (known as "dry" physics) in order to suppress shallow fast-growing structures near the surface, which are not of interest because they are strongly damped in the non-linear integrations. Nowadays, the TLM linearized physics can account for vertical diffusion, gravity-wave drag, radiation, deep convection and large-scale condensation, the last two being known as "moist" physics. SVs computed using TLM that include moist physics are known as "moist" SVs, the opposite SVs being known as "dry" SVs. Two other important choices that must be made in computing SVs regard the TLM horizontal resolution and OTI. In the following, we present a brief description of the structure and characteristics of dry and moist SVs, followed by a review regarding the SVs sensitivity to the choice of TLM resolution and OTI.

4.1. Dry extratropical SVs

SVs structure depends on the norm chosen, various choices of the initial norm leading to different initial structures and evolutions. Because total energy represents the most commonly used norm, in the following we describe the structure of SVs computed with dry total-energy norm.

Usually the leading extratropical SVs have at initial time a westward tilt with height and a meridional phase tilt that diminish with time (e.g. Buizza, 1994; Montani and Thorpe, 2002; Coutinho et al., 2004). The vertical westward tilt indicates baroclinically unstable perturbations that favor the conversion of available potential energy into kinetic energy, while the meridional tilt against the horizontal shear denotes a barotropic mechanism for SV growth characterized by the transformation of basic-state kinetic energy into the perturbation kinetic energy. Fig. 1 presents an example of horizontal (c and d) and vertical (a and b) structure for a typical total-energy extratropical SV. This SV represents the leading SV from a set of ten SVs that was computed using the TLM of Canadian GEM model with an OTI of 36 hours and a final-time norm restricted to a region of the North American Continent. The basic state and the TLM had a horizontal resolution of 1° and 28 levels in the vertical. The ICs correspond to 5 December 1992 at 00:00 UTC. The initial- and final-time norms are the dry total-energy norms (as defined in Diaconescu et al., 2012) and the TLM includes the linearization of dynamical GEM core and a vertical diffusion scheme. Fig. 1a and c shows the temperature field at initial time, while the temperature field at final time can be visualized in Fig. 1b and d. In 36 hours, the perturbation grew in amplitude and changed its shape: the vertical westward tilt changed into a slight eastward tilt and the horizontal tilt has disappeared. Usually, the same initial-time vertically tilted pattern characterizes the leading SVs in terms of wind or potential vorticity (PV) (see Montani and Thorpe, 2002 for the SV structure in terms of PV).

The total-energy partitions into the kinetic, potential and surface-pressure components for this set of first ten SVs at initial and final times are represented in Fig. 2. The panels show that the ratio of kinetic to potential energy of SVs is approximately 1:3 at initial time and 5:1 at final time. The surface-pressure term represents only a small percentage of the total energy. Usually the total-energy middle-latitude SVs is characterized by a dominant potential energy at initial time and a dominant kinetic energy component at final time (e.g., Gelaro et al., 1998; Zadra et al., 2004; Diaconescu et al., 2012). The transformation from initial potential to final mainly kinetic energy can be interpreted as the rotation of the off-attractor initial-time SVs toward the on-attractor final-time SVs by adjustment processes. Diaconescu et al. (2012) presented the 36-hour time evolution of the total-energy components for a typical extratropical leading SV and showed that except at initial time, all other steps are characterized by the dominance of kinetic energy.

Other important information can be depicted from the total-energy vertical profile. In Fig. 3, we display the average total-energy vertical profile computed as the mean of the ten extratropical SVs (from the set presented in Fig. 2) total energy horizontally integrated over the globe. It can be seen that at initial time (dashed line), the energy maximum is located in the middle troposphere. Several studies have shown that dry total-energy SVs is usually located in the lower and middle troposphere at initial time (e.g. Buizza and Palmer, 1995; Montani and Thorpe, 2002; Coutinho et al., 2004; Zadra et al., 2004). During their growth, there is generally an upward energy transfer toward the jet level, sometimes accompanied also by a downward energy transfer toward the surface as can be seen in Fig. 3 (solid line). The initial-time location is also a function of OTI: long OTIs yield SVs that initially have a lower location comparatively to shorter OTIs, which favor mid-troposphere structures. According to Coutinho et al. (2004), for a long OTI, the direct interaction with the surface tends to inhibit the initial growth and gives more distance for upward propagation and growth.

Montani and Thorpe (2002) used PV diagnostics to investigate the total-energy SV growth. They showed that the growth is usually greater at the tropopause where the perturbation velocity components can interact effectively with the basic state and grow. By separating the perturbation in two parts, above and below the 500-hPa level, they found that the perturbations initially confined at low levels can interact with the upper-level basic-state fields more efficiently than those localized above 500 hPa. These results confirm the study of Badger and Hoskins (2001) who, in the framework of a simplified Eady model, also identified the lower troposphere as the location where an initial perturbation can experience rapid growth. Montani and Thorpe (2002) found that the final-time energy could also increase significantly at low levels by normal-mode-like growth through PV coupling, leading to near-surface perturbations. The energy growth at low levels has often the main final-time peak located just above the boundary layer as can be seen in Fig. 3.

The energy spectra bring other information about the SV structure. Fig. 4 (corresponding to Fig. 3c and d from Zadra et al., 2004) shows the initial-time and final time energy spectra, averaged among the first 45 SVs computed using the GEM TLM with a resolution of 3°, 28 levels in the vertical, and an OTI of 48 hours. The final-time dry total-energy norm was restricted to latitudes north of 30°N and the ICs were taken from the analysis of 16 February 2002. The energy spectra show an upscale energy transfer with a pronounced final-time spectral peak around wavenumbers 12–14, which is consistent with baroclinic disturbances at synoptic scales as noted in other studies (e.g. Buizza and Palmer, 1995; Gelaro et al., 1998; Buehner and Zadra, 2006). This upscale energy transformation is one of the total-energy extratropical SV characteristics that distinguish them from the leading Lyapunov

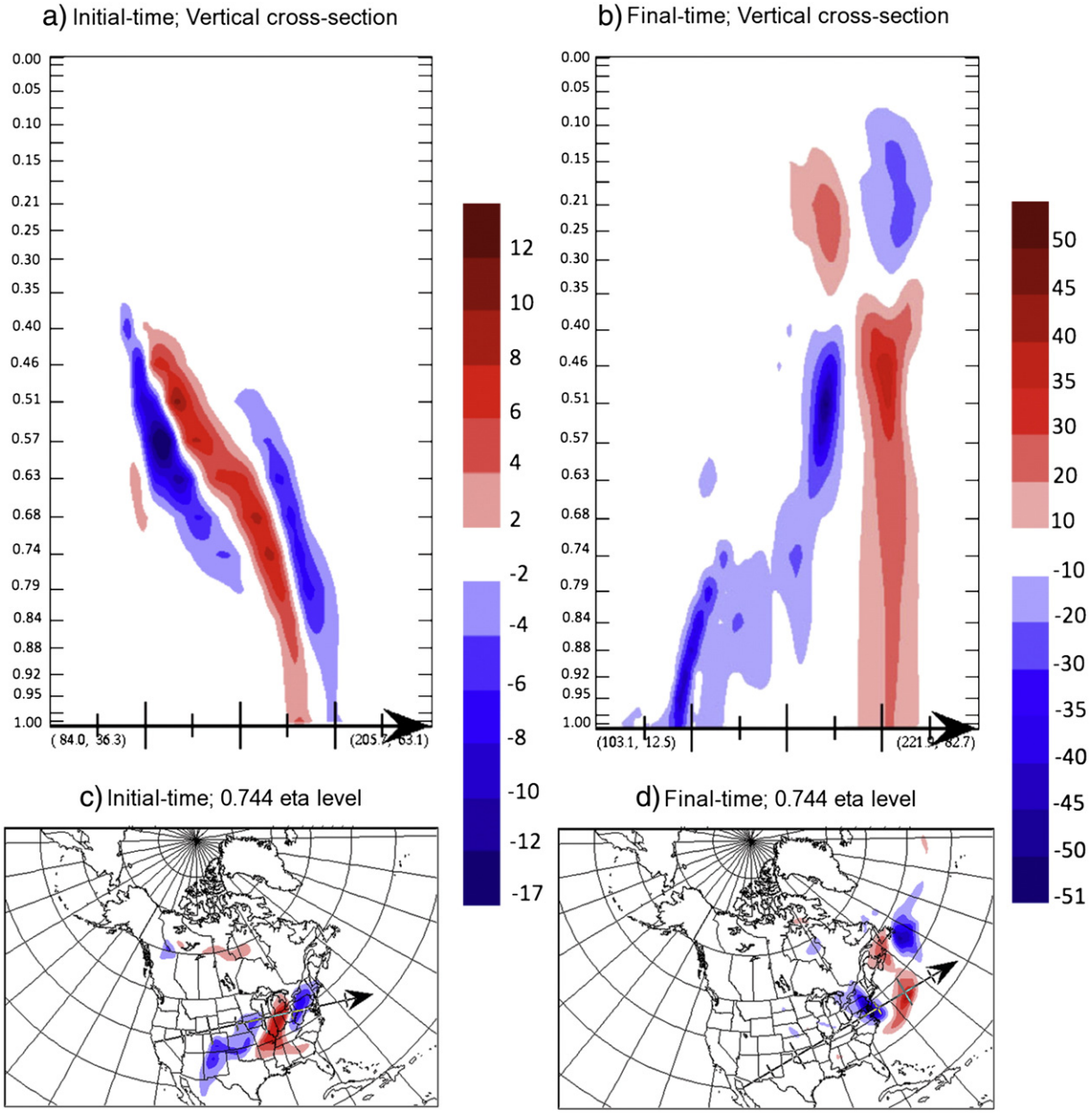

Fig. 1. (a and b) Vertical cross-section and (c and d) horizontal cross-section at the 0.744 eta level of the temperature field corresponding to the first singular vector at (a and c) initial time and (b and d) final time. The arrow indicates the region of the vertical cross-section. Note the different contour intervals between the (a,c) and (b,d) panels.

Vectors that have fixed structure during their time evolution (hence fixed spectra) and amplitude growing exponentially with time.

As previously mentioned, SVs structure depends on the norm. Barkmeijer et al. (1999) compared the 3D-Var Hessian SVs with total-energy SVs and found that the initial-time Hessian SVs differ considerably from the total-energy SVs. Fig. 5 (corresponding to Fig. 1 from Barkmeijer et al. (1999)) shows the total-energy spectrum and the total-energy vertical distribution for the total-energy SVs and Hessian SVs. The initial-time Hessian SVs have much more power at large scales and are located especially at the upper levels as the final-time Hessian SVs. No upscale energy transfer is observed for Hessian SVs and their amplification is much slower. However, the authors remark that despite these differences, the leading 25 total-energy SVs and Hessian SVs explain nearly the same part of the two-day forecast error. This is due to the fact that both the Hessian SVs and the total-energy SVs are evolving toward the Lyapunov Vector. The fact that the Hessian SVs have the same shape at initial and final times and smaller growth rates, suggests that, unlike the initial-time total-energy SVs, they are on the attractor at initial time, and thus represent real atmospheric perturbations.

4.2. Moist SVs

The importance of including moist processes in the computation of SVs was underlined by numerous papers (e.g., Ehrendorfer et al., 1999; Coutinho et al., 2004; Zadra et al., 2004; Hoskins and Coutinho, 2005 for extratropical SVs; and Barkmeijer et al., 2001; Kim and Jung, 2009a for tropical SVs). In this section we summarize the primary effects of moist physics on SVs.

Ehrendorfer et al. (1999) analyzed the effect of moist physics on extratropical total-energy SVs in the context of the National Center for Atmospheric Research (NCAR) Mesoscale Adjoint Modeling System

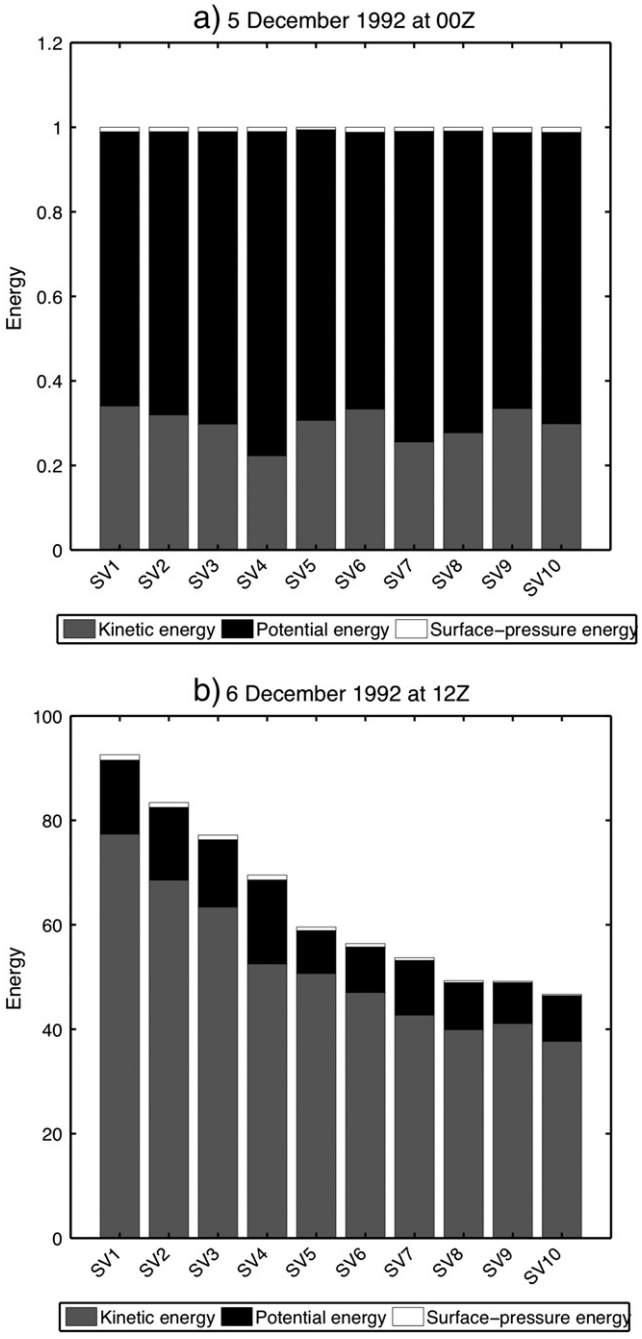

Fig. 2. Energy partition in kinetic (gray), potential (black) and surface-pressure (white) terms at (a) initial and (b) final time, with initial-time total energy normalized as one.

(MAMS2). Two important properties were highlighted in their study. First, they show that a moist TLM leads to faster growth compared to the case in which only dry processes are considered. Secondly, there are new growing SVs that appear in the case of a moist TLM compared to a dry TLM. Hence, the moist processes not only modulate the dry SVs but they also add new mechanisms of error growth. The new SVs have maxima located in the lower troposphere and growth rates much larger than the growth rates of the dry SVs. These results highlight the necessity of a moist TLM in order to capture all structures that might potentially grow in a moist environment.

Another important concern is the choice of a norm that accounts for the moist part of SVs and its impact on SVs spectrum. Ehrendorfer et al. (1999) have used an extension of the widely employed dry total-energy

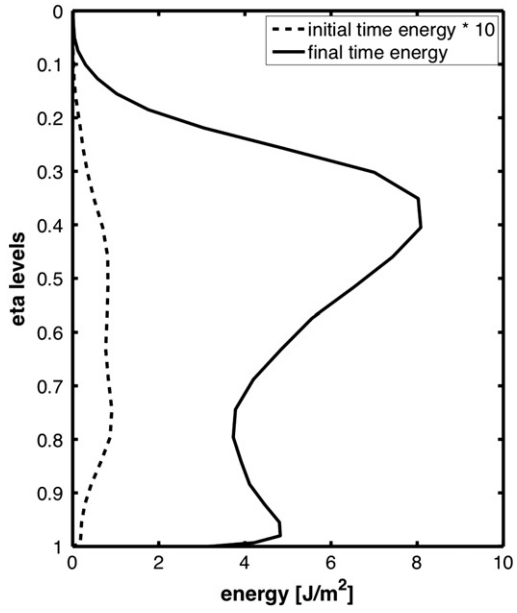

Fig. 3. Vertical distribution of the final-time (solid line) and initial-time (dashed line) total energy averaged among the first ten SVs. For clarity, the initial-time total energy has been multiplied by 10.

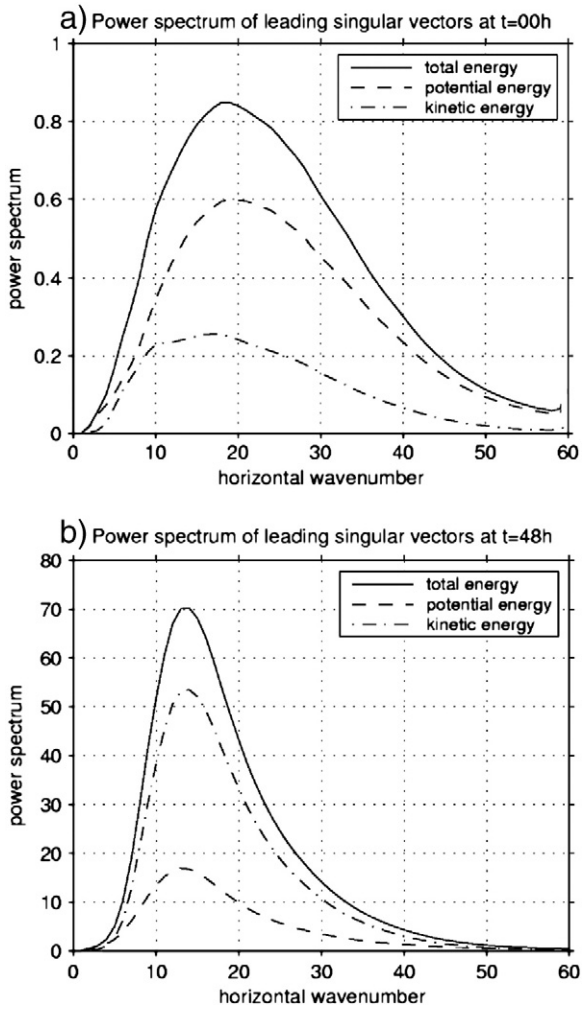

Fig. 4. The potential (dashed line), kinetic (dot-dashed line) and total (solid line) energy spectra at (a) initial and (b) final times, averaged among the first 45 SVs.
Source: Zadra et al. (2004); © Crown copyright, 2004.

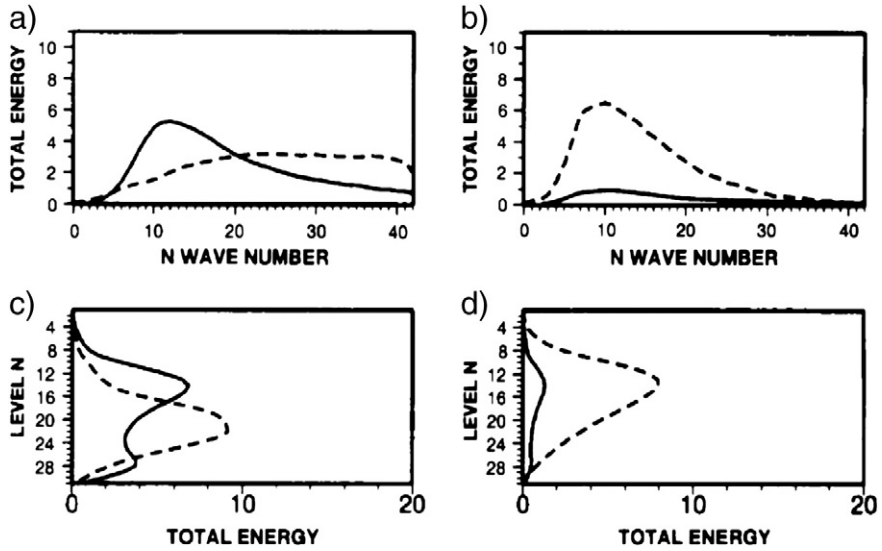

Fig. 5. (a and b) Spectrum and (c and d) vertical distribution of the total energy for the (a and c) total-energy SVs and (b and d) Hessian SVs. Values at initial (final) time are given by dashed (solid) lines. The total energy at initial time has been multiplied by 100.
Source: Barkmeijer et al. (1999); © Crown copyright, 1999.

norm by adding a quadratic term based on the physical effect of condensation/evaporation on temperature:

$$E_m = \frac{1}{2}\frac{1}{A}\int_A \int_0^1 \varepsilon \left[\frac{L_c^2}{c_p T_r} q^2\right] d\eta dA. \quad (21)$$

Here, q is the mixing ratio, T_r a reference temperature, c_p is the specific heat at constant pressure and L_c is the latent heat of condensation per unit mass. The constant ε is use to give different weights to the humidity term. The integral extends over the full horizontal domain A and vertical direction η. They found that the leading subspaces for dry and moist total-energy norms are quite comparable and that the growth rates depend more on the choice of the basic state and linearized model (moist versus dry TLM) than on the choice of the norm (moist versus dry total-energy norm).

Zadra et al. (2004) computed also wintertime extratropical SVs with the dry and moist TLM of Canadian Global Environmental Multiscale (GEM) model and analyzed the impact of four parameterizations (vertical diffusion, subgrid-scale orographic drag, stratiform and convective precipitation) on the SV properties. They showed that the most significant impact was given by the stratiform precipitation and that the convective precipitation had only a small impact for wintertime extratropical SVs. Generally, the moist physics enhances the SV growth, shifts the energy to smaller scales and intensifies the energy transfer to the jet level. Similar results were obtained by Coutinho et al. (2004) and Hoskins and Coutinho (2005) using the dry and full physics TLM of ECMWF.

They point out that the moist extratropical SV vertical structure is similar to the dry SV structure, both presenting a westward tilt with height. Coutinho et al. (2004) noted also that in general, the moist structures show less evidence of a horizontal tilt and therefore of barotropic conversion. The SVs computed with moist processes have a tighter and deeper structure and they peak at shorter wavelengths. This can be seen in Fig. 6 (Fig. 2 from Coutinho et al., 2004), which presents the initial- and final-time total-energy spectra averaged among the first ten SVs for experiments with dry and moist TLMs at two horizontal triangular spectral truncations (T42 and T63) and two OTIs (24 and 48 hours). The shift to higher wavenumbers is more evident for the experiment with a higher resolution. Hence the use of a TLM with high horizontal resolution is necessary in order to reveal all small-scale structures that might grow rapidly in a moist model.

In their study, Kim and Jung (2009a) compared the dry and moist tropical SVs computed with the Pennsylvania State University—NCAR Mesoscale Model (MM5) TLM at 100-km horizontal resolution and with dry and moist total-energy norms. As in the case of extratropical SVs, moist physics increase the growth rate of tropical SVs and cause smaller horizontal structures located in the lower troposphere. However, the initial-time tropical SVs energy is dominated by the vorticity component and not by the potential component. Fig. 7 (corresponding to Fig. 11a, b, i and j from Kim and Jung, 2009a) plots the vertical distribution of energy for the leading SV at initial and final time, for the experiments with dry and moist total-energy norms and TLMs. When the moist total-energy norm with full weighting ($\varepsilon = 1$) is used (Fig. 7b), the initial-time kinetic and potential components are transformed in the dominant humidity component at final time. Similar results were obtained by Barkmeijer et al. (2001), who analyzed the tropical moist SVs using the global ECMWF TLM at T42 horizontal resolution. They mentioned also that in the case of SVs computed for tropical cyclone (TC) prediction, the choice of the target area is crucial in determining the location and properties of SV because a large target area results in many SVs that are not located in the cyclone area. Puri et al. (2001) studied the ECMWF tropical SVs in terms of the spread in cyclone tracks and intensities; they noted also that larger target areas lead to reduced spread and therefore to a reduced potential value for the forecast. However, for small target areas, a much larger spread is obtained. Kim and Jung (2009a) have used a small target area located on the TC center. They remarked that even for such a small target area, the moist SVs have relatively stronger sensitivity in the vicinity of a TC than the dry SVs, which usually have remote locations from the TC center associated for example with a mid-latitude trough.

4.3. The TLM horizontal resolution and the OTI

Besides the norm, there are two other important parameters that must be chosen when computing SVs: the TLM horizontal resolution and the OTI. Several studies have focused on the analysis of the SV sensitivity to the choice of these two parameters (e.g. Buizza, 1994, 1998; Komori and Kadowaki, 2010).

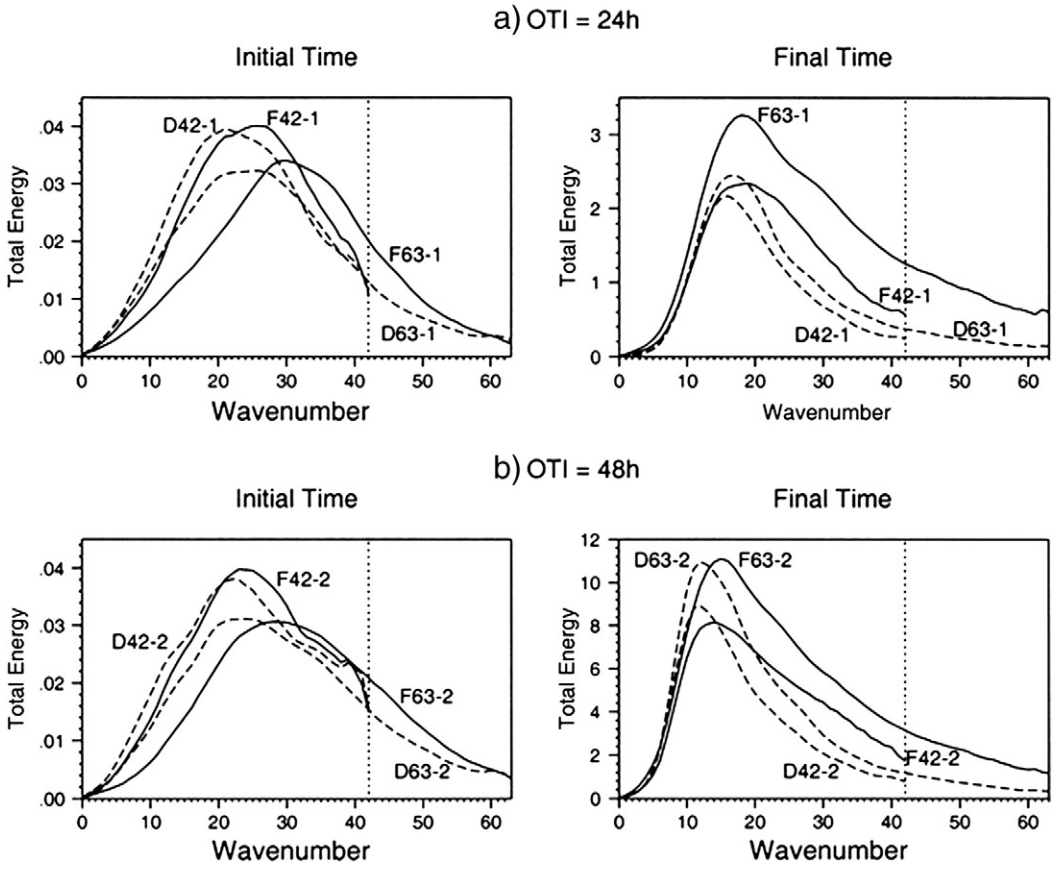

Fig. 6. The total-energy spectrum averaged among the first 10 SVs for experiments with dry physics (dashed lines) and full physics (solid lines) at initial time (left) and final time (right) at OTI of (a) 24 h and (b) 48 h.
Source: Coutinho et al. (2004); © 2004 American Meteorological Society.

As mentioned in the previous section, Coutinho et al. (2004) used dry and moist TLMs with two different horizontal triangular spectral truncations (T42 and T63) for computing extratropical SVs. Their results showed that the use of a moist TLM requires a higher horizontal resolution in order to detect moist perturbations that have small-scale characteristics. Buizza (1998) also computed extratropical SVs using ECMWF dry TLM at three different horizontal spectral truncations (T21, T42 and T63). He compared the corresponding SV subspaces to the forecast error and found that T42 and T63 SVs capture better the forecast error scales in eight out of eleven cases. The fact that T63 SVs do not outperform T42 SVs could indicate that more physical processes must be included in the tangent model versions at higher resolution. Nowadays, the operational ECMWF EPS uses a T42 dry TLM for computing extratropical SVs (Palmer et al., 2007).

In a recent paper, Komori and Kadowaki (2010) found that the TLM resolution has a great impact on the structure of dry tropical total-energy SVs targeted on TCs. First it was found that the shift towards higher wavenumbers is much clearer in the case of a higher horizontal resolution. Secondly, different resolutions emphasized different phenomena in the structure of the leading SVs. Fig. 8 (corresponding to Fig. 2 from Komori and Kadowaki, 2010) shows the total-energy horizontal distribution for the initial-time leading SV computed using a dry TLM with three horizontal resolutions: TL63, TL95 and TL159. At TL63, the energy has two maxima: the primary maximum is located northwest from the TC center and is associated with the upper-level mid-latitude trough; the secondary maximum is placed in the TC surrounding area, in the low troposphere. At TL159, the primary maximum is located on the east side area of the cyclone, while the upper-level structure is very much reduced. The authors concluded that a certain degree of resolution in the TLM and ADM is required to properly detect sensitive areas around the TC.

It can be concluded that a higher horizontal-resolution TLM is desirable especially in the case of tropical SVs computation. However, given the high cost of a high-resolution TLM, the operational ECMWF uses in ensemble prediction of TC only the first five moist SVs computed at T42, for up to six tropical optimization regions. The moist total-energy norm is limited between surface and 500 hPa, emphasizing on the surface maximum that is associated with TC (Puri et al., 2001; Palmer et al., 2007; Buizza, 2010).

Concerning the SVs sensitivities to different OTIs, Buizza (1994) has analyzed the impact of OTI on extratropical SVs computed with T21 dry TLM with initial amplitudes comparable with analysis-error estimates, and he found similar SVs for OTIs varying between 24 and 72 hours. On the other hand, Komori and Kadowaki (2010) compared the TL159 dry tropical SVs targeted to TC for two different OTIs: 24 h and 48 h. They found that the 48 h SVs have a larger influence from mid-latitude troughs than the 24 h SVs, which are located mostly in the TC surrounding flow. This indicates that the large-scale mid-latitude structures need longer OTI to develop, while the SVs surrounding the TC have a more rapid growth and a shorter OTI will emphasize them.

The choice of OTI is related to the question of the validity of the tangent linear approximation. The fact that SVs are computed in a linear approximation context puts an upper bound on OTI fixed by the approximation validity. This is usually tested by comparing the growth of SVs in the full non-linear model and in the TLM. Buizza (1994) highlighted an upper limit for OTI of the order of 48 hours for the dry extratropical SVs at T21.

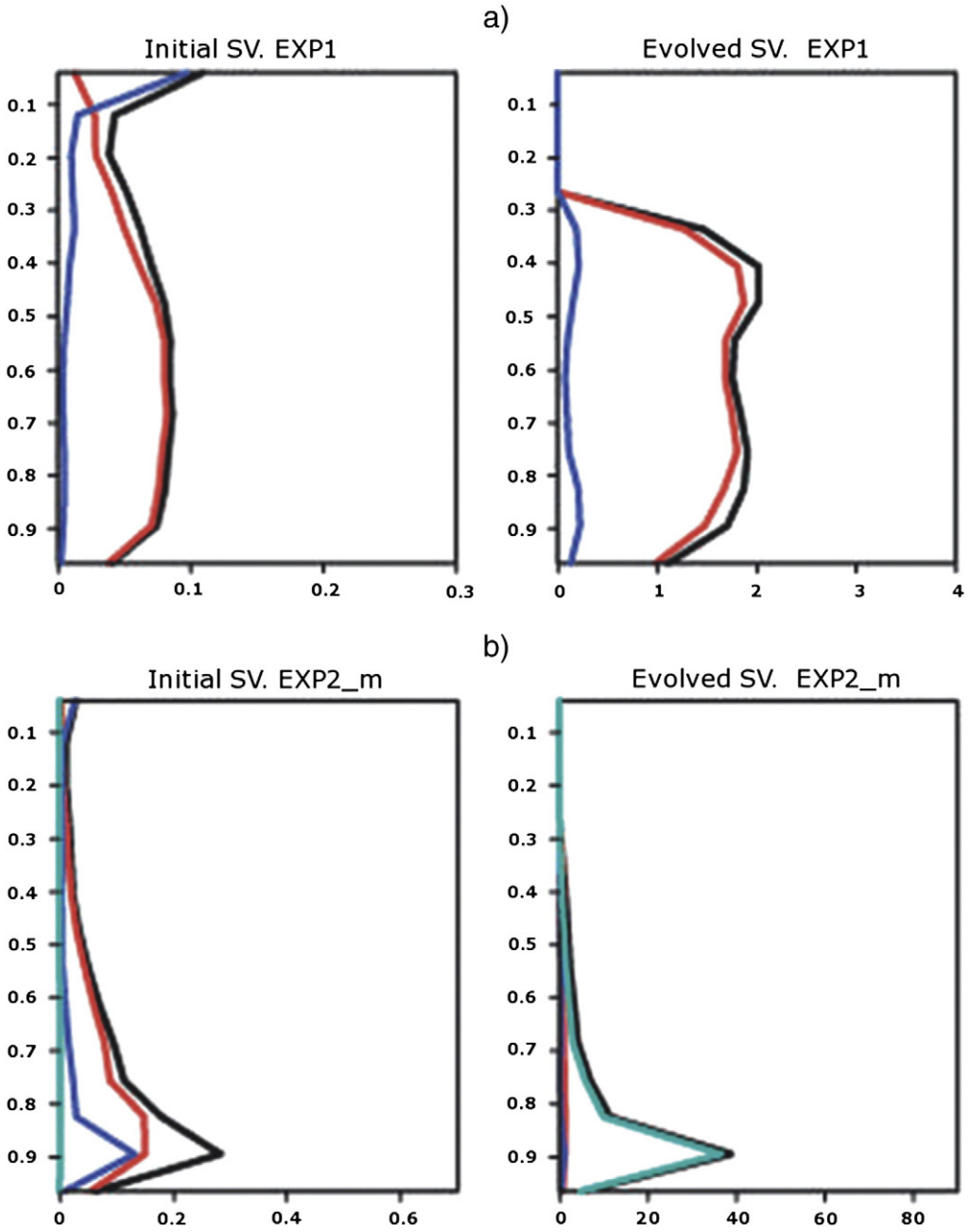

Fig. 7. Initial and evolved leading SV energy vertical distribution (J/kg) for (a) dry TLM with dry total-energy norm and (b) moist TLM with moist total-energy norm with full weighting ($\varepsilon = 1$). The total energy is represented in black, kinetic energy in red, potential energy in blue and the moist energy in cyan.
Source: Figure adapted from Kim and Jung (2009a); © 2009 American Meteorological Society.

However, Tanguay et al. (1995) pointed out that the TLM validity depends on the resolution. Generally a higher resolution implies a reduction of the TLM validity. Reynolds and Rosmond (2003) showed also that the TLM validity is a function of scale and norm. Their study indicated that the linear assumption for small scales is broken after 12 hours, while the large scale remain significantly linear up to two or three days. As mentioned before, the moist SVs have higher growth rate and present smaller-scale structures. In their conclusion, Reynolds and Rosmond (2003) pointed out that, despite the fact that a moist TLM is a more accurate representation of the full non-linear model, its results can be less relevant for small scales because of non-linearities that dominate the small scales of the full model. Errico and Raeder (1999) analyzed the accuracy of a moist TLM and adjoint model; they found that the tangent linear assumption is quantitatively accurate for OTI of 24 hours in regions of significant dynamical forcing (therefore with large-scale structures), but only qualitatively accurate in regions dominated by moist convection, which usually presents small-scale structures.

We note that most SVs studies use an OTI of 48 hours for dry SVs and an OTI of 24 hours for moist SVs.

5. Applications

5.1. General information

SVs are employed for many types of applications in atmospheric science. Such applications include forecast error estimation, predictability studies and growth arising from hydrodynamic instabilities, ensemble forecasting and targeted adaptive observations. These applications are

based principally on the fact that SVs form a complete basis of orthonormal structures ordered according to growth potential. Hence, as indicated in Ehrendorfer and Errico (1995), any arbitrary initial perturbation ($x(t)$) can be decomposed in terms of this complete basis by projecting the perturbation in the directions of SVs:

$$x(t) = \sum_{i=1}^{N} \alpha_i \hat{y}_i(t) \tag{22}$$

$$\alpha_i = \langle x(t), E\hat{y}_i(t) \rangle \tag{23}$$

Here, $\hat{y}_i(t)$ are the SVs with unity norm, α_i are the respective projection coefficients and E is the norm at time t. Therefore, the perturbation amplitude can be written as

$$|x(t)| = \sqrt{\|x(t)\|^2} = \sqrt{\sum_{i=1}^{N} \alpha_i^2} \tag{24}$$

The complete basis of SVs contains growing, neutral and decaying SVs. In their study on the spectra of singular values in a regional model, Errico et al. (2001) used several sets with a very large number of SVs; they showed that a large part of SVs are slowly growing or decaying SVs, and that only a small fraction of the SVs are very fast-growing structures. As a consequence, for the arbitrary perturbation expressed in Eq. (24), future growth is expected only if the magnitudes of the projections on the growing SVs are sufficiently large with respect to those for decaying SVs. Because the number of slow growing SVs is very large, knowledge of the full spectrum of growing SVs (or the most part of it) should be of interest when studying growing atmospheric perturbations.

Due to computational cost constraints, most studies with complex models use subsets of SVs limited to the first 5 to 50 most rapid SVs, out of a possible set of 10^6–10^7 or more. In their study on SV sensitivity to the horizontal resolution, Buizza (1998) considered a set with only the first ten fastest growing SVs. The 10-dimensional subspace of the system's phase space at time t spanned by these SVs is:

$$G(t) = \left\{ \hat{y}_j(t), j = 1, 10 \right\} \tag{25}$$

Only the fast-growing part ($\tilde{x}(t)$) of an arbitrary perturbation ($x(t)$) will project into this subspace:

$$\tilde{x}(t) = \sum_{j=1}^{10} \alpha_j \hat{y}_j(t). \tag{26}$$

The ratio between the norms of the projected part and the full perturbation is usually used to measure the part explained by the most rapid SVs:

$$p(t) = \frac{\|\tilde{x}(t)\|^2}{\|x(t)\|^2} \tag{27}$$

This ratio is called the projection index.

5.2. Forecast error estimation

Buizza (1998) used the projection index to find the proportion in which the final-time leading ten SVs, computed with ECMWF TLM at T21, T42 and T63 horizontal resolution, can explain the two-day forecast errors for the period of 3 to 13 September 1993. The projection indices were rather small, with values between 20% and 45% and an average of 28%, suggesting that more than ten SVs are needed to

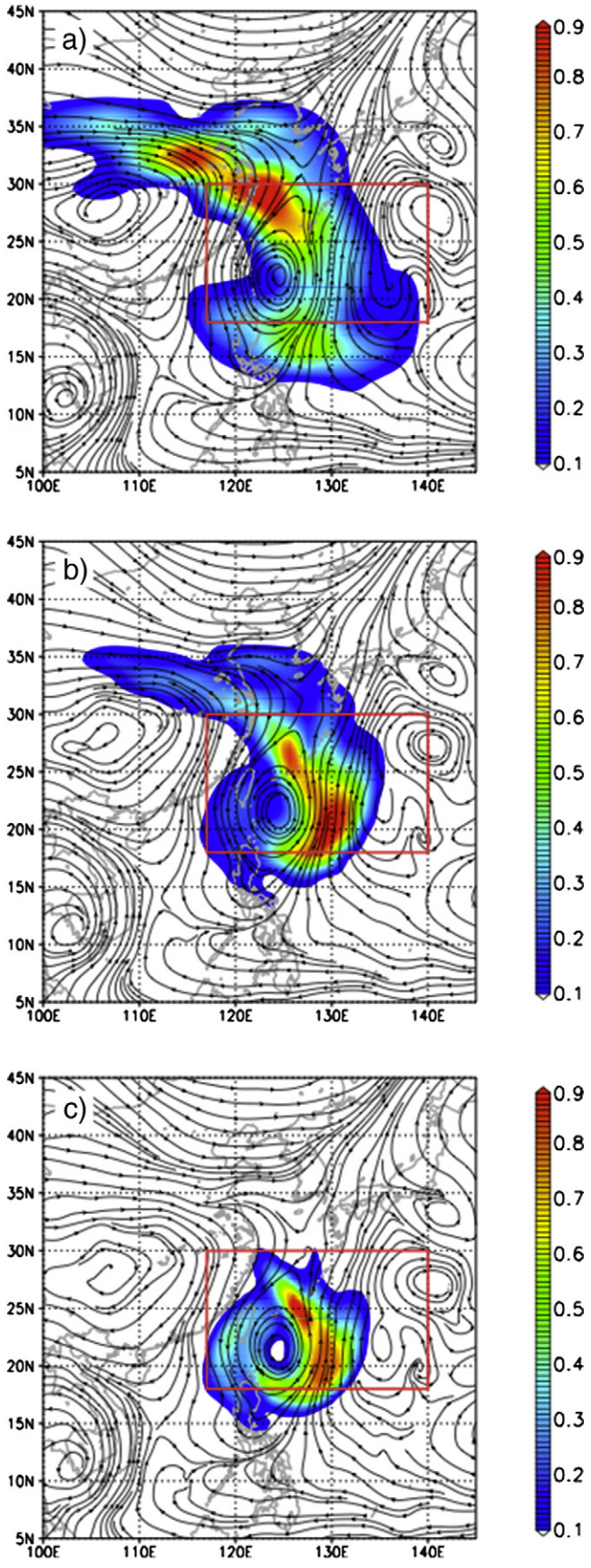

Fig. 8. Vertically integrated total energy for the initial-time leading SV superimposed on the analyzed streamlines at 500 hPa. The SVs are computed with JMA TL/AD model at a resolution of (a) TL63L60, (b) TL95L60 and (c) TL159L60. The red rectangle represents the target area.
Source: Komori and Kadowaki (2010); ©2010, the Meteorological Society of Japan.

describe the forecast error. A larger percentage was obtained by Barkmeijer et al. (1999) who projected the operational two-day forecast error onto 25 final-time Hessian SVs and 25 final-time total-energy SVs. Both types of SVs described nearly the same fraction in terms of total energy, which varies for the ten cases analyzed between 30% and 60%. However, there were other cases when a set of 25 total-energy SVs explained a very small percentage of two-day Northern Hemisphere forecast error. For winter cases, Barkmeijer et al. (2003) obtained percentages varying between 0.1 and 0.22, while for summer cases the percentages had values between 0.08 and 0.19.

In their study, Gelaro et al. (1998) compared a set of 30 SVs to the analysis-error field and to the forecast error sensitivity pattern obtained from an adjoint model integration. They showed that the 30 evolved dry-total-energy SVs at T42 resolution captured a large fraction of the covariance of the Northern Hemisphere sensitivity pattern in most of the cases examined. Gelaro et al. (1998) have grouped the analyzed cases into two categories: cases when the forecast had a low skill and cases when the forecast had an average skill. They pointed out that fewer SVs were needed in the low-skill cases than in average-skill cases. It is important to note that in the average-skill cases, the patterns were less localized and the projection was made onto the slowly growing final-time SVs and not on the leading SV, while the projection for the low-skill cases is dominated by the leading final-time SVs.

5.3. Predictability studies and growth arising from hydrodynamic instabilities

SVs have been also employed to study the growth of perturbations in the atmosphere or oceans in order to explain a particular phenomenon. For example, Diaconescu et al. (2012) used a set of ten SVs in the analysis of the internal variability of a Regional Climate Model (RCM). Their objective was to find in which proportion the growth noted in the model internal variability (i.e. the dispersion of 21 RCM simulations with different initial conditions) was due to rapidly growing perturbations developing in dynamically unstable regions. The ensemble of RCM simulations was expressed in terms of perturbations from a reference simulation and then the RCM perturbations were projected onto a set of SVs computed with initial conditions from the RCM reference state. They found that the projections on SVs at initial time were very small. However, these projections grew rapidly during the next 36 h and ended up representing an important part of the RCM-perturbation total energy. A high structural similarity was found between the RCM perturbations and the first SV after 24- to 36-h of the tangent linear model integration. The projection was made in a large proportion at final time on the first SV, while for the nine remaining SVs only small projections have occurred. The overall picture showed that the subspace of ten SVs accounted for over 70% of the RCM IV growth in 36 h for the case analyzed.

Another example is the study of Cheng et al. (2010), who used SVs to study ENSO predictability for a period of 148 years. They have computed SVs for the Zebiak–Cane model of the tropical Pacific coupled ocean–atmosphere system with an OTI of nine months for the sea surface temperature (SST) field; they found that the SST of the coupled leading SV has a west–east dipole structure oriented across the tropical Pacific, with one center of action located in the east Pacific and the other in the center Pacific. Their analysis was limited to only the first SV and small correlation has been found between the leading SV growth rate and ENSO predictability at interannual time scales.

Descamps et al. (2007) used SVs to verify if generalized linear baroclinic instability can explain the cases of mid-latitude cyclogenesis. By subtracting a cyclone and its precursors from a basic state and comparing it with a set of ten SVs computed using dry total-energy norms and OTI of 24 hours corresponding to the incipient stage of cyclogenesis, they found that the structure of a single SV has little to share with that of a real cyclone.

Other studies used SVs not to explain the cyclogenesis but to identify sensitive regions that can influence the evolution of a TC. A better understanding of these processes could help in future improvements of TC forecasts. An example is the study of Chen et al. (2009) who used SVs to obtain information about the dynamical processes that have an important impact on TC evolution. The composites for 72 cases with TCs show that the maximum initial-time SV is located at around 500 km from the center. Other initial-time SVs are situated in confluence regions generated by several systems such as the mid-latitude jet, the subtropical high and the TC. Therefore, it highlights these regions as areas with a delicate balance that influences the evolution of several synoptic systems. Kim and Jung (2009b) and Reynolds et al. (2009) also used SVs to examine TC sensitivity during recurvature and the subsequent downstream impacts resulting from the interaction of the TC with the mid-latitude environment. They showed that the SVs situated in mid-latitude upper trough region become dominant as the TC recurves, while the SVs close to the TC center play an important role when the TC is far from recurvature. Kim and Jung (2009b) pointed out that the sensitive area around the TC center is associated with warming in the mid-troposphere, while the sensitivity area under the upper trough are associated with strong baroclinicity and frontogenesis. Most of the initial-time remote SVs evolve to mid-to-lower troposphere structures that are co-located with the TC at final time.

5.4. Ensemble prediction systems

There are two primary error sources in forecasts: errors in the estimation of the initial model state and errors due to imperfections in the model formulation. These errors can grow with time and limit the skill of a single forecast. The purpose of ensemble forecasts with perturbed initial conditions is to quantify the forecast uncertainty (forecast-state errors) caused by initial conditions uncertainty (initial-state errors), in the perfect model assumption. In principle, the statistical properties of initial-state errors can be described in terms of a high-dimensional probability density function (pdf) (e.g. Houtekamer, 1995). The main goal of ensemble forecast initialization methods is to adequately sample the initial-state pdf. Furthermore, the resulting initial states are evolved using the model and result into an ensemble of forecasts. In the perfect model assumption, a proper sample of the initial-state error pdf will result in a proper sample of the forecast-state error pdf. In practice, the initial condition errors are inseparable from model errors and they must be considered jointly (Leutbecher and Palmer, 2008).

Several methods can be used to deal with the uncertainty in initial conditions. The most popular are: the methods of SVs, the breeding of growing modes, ensemble Kalman filter and ensemble transform Kalman filter. The breeding of growing modes is described in detail in Toth and Kalnay (1997). The ensemble Kalman filter and ensemble transform Kalman filter are ensemble-based data-assimilation approaches and an introduction at these methods can be found in Zhang and Pu (2010). The SVs method was developed at ECMWF and is used presently in several NWP centers. A detailed description of the use of leading SVs in the ECMWF EPS can be found in Molteni et al. (1996) and information about the later developments of ECMWF EPS are presented in Buizza et al. (2007a, 2008), Palmer et al. (2007) and Leutbecher and Palmer (2008). In the following, we summarize the main points of the ECMWF's medium-range EPS configuration used in Leutbecher and Palmer (2008) and Isaksen et al. (2010).

In NWP, the initial state of the atmosphere is estimated using data-assimilation methods. ECMWF EPS presented in the last two papers uses a four-dimensional variational assimilation system, which blends information from observations with that from the most recent forecast. As consequence, the initial-state errors are the result of complex interactions between growing parts of past forecast errors and the reduction of those errors during the current data-assimilation cycle.

The SVs method assumes that, from all initial-state errors, the fastest growing ones are responsible for a large part of the forecast

uncertainty. These fast-growing perturbations can be obtained by computing the leading initial-time SVs. In ECMWF EPS, there are 50 leading initial-time SVs that are computed for each extratropical hemisphere using the dry T42L62 TLM, an OTI of 48 hours and total-energy initial- and final-time norms. The non-linear trajectory is started from a six-hour forecast initialized 6 hours in advance. ECMWF EPS does not compute SVs over the entire tropical region. Instead of that, the SVs are targeted to up to 6 regions with active TCs. For each of these regions, the first 5 SVs are computed with a moist TLM and a norm confined to the levels below 500 hPa and targeted to the regions where the tropical storms are developing. The TC targeted SVs are computed in the subspace orthogonal to the extratropical SV space. Once computed, SVs are linearly combined using a Gaussian sampling technique and re-scaled to create perturbations that cover most of the targeted regions without overlap, and to have amplitude comparable with analysis-error estimate from the high-resolution data-assimilation system.

The ensemble skill is improved if at those perturbations are added other perturbations that represent the errors that have been growing during the current and past data-assimilation cycles; these perturbations will reflect the analysis uncertainty. Before June 2010, the past-grown errors' part of the perturbation was computed using 48-h linearly evolved SVs computed 48-h prior to the ensemble start time (Leutbecher and Palmer, 2008). After June 2010, the evolved SVs were replaced by perturbations based on an Ensemble of Data Assimilation (EDA), which permits to quantify the analysis uncertainty by taking into account the model dynamics. The use of EDA-based perturbations improved the EPS skill, especially in the tropics (e.g. Buizza et al., 2008; Isaksen et al., 2010).

Hence, after June 2010, the initial conditions perturbations of the ECMWF EPS are computed using EDA-based perturbations and a linear combination of initial-time leading SVs. ECMWF EPS uses 25 pairs of such perturbations that are added and subtracted from the operational analysis leading to 50 perturbed members. The 51st member is a non-perturbed forecast, which is started from the operational analysis (at the EPS resolution). By using pairs of opposing perturbations, the mean of the ensemble is initially identical to the non-perturbed member.

The Japan Meteorological Agency (JMA) runs ensemble prediction systems derived from the TL319 global model that also use SVs to perturb the initial conditions provided by the 4D-Var analysis:

(1) The One-Week Ensemble Prediction System (WEPS) once a day with 51 members;
(2) The Typhoon Ensemble Prediction System (TEPS) four times a day with 11 members.

The main difference between WEPS and ECMWF EPS consists in the targeted areas. In WEPS, moist SVs are targeted for the whole tropics and the dry SVs are targeted only for the northern hemisphere.

The TEPS became operational in February 2008 and has an aim to improve track forecast targeting for TCs in the western North Pacific and the South China Sea. For one forecast event, up to forty total-energy SVs are computed using TLM at T63 resolution and OTI of 24 hours:

(1) Ten dry SVs targeted for the mid-latitude;
(2) Up to thirty moist SVs targeted for up to three TCs at a time.

The moist SVs are targeted to a rectangle of 10° in latitude and 20° in longitude with its center at the forecast TC's central position. A detailed description of the JMA TEPS is given in Yamaguchi and Komori (2009).

Other forecast centers that use SVs to initialize ensemble forecasts are Météo-France and Bureau of Meteorology (BoM) in Australia.

5.5. Targeted observations

SVs are also employed in targeted (adaptive) observations. Target observation strategies aim at identifying regions where additional observations have the potential to significantly improve weather forecasts. Changes to the initial conditions in these "sensitive" regions are expected to have a larger effect on the forecast skill than changes in other regions (Kim and Jung, 2009a).

Several strategies have recently been proposed to evaluate the impact of targeting observations on the quality of forecasts (Rabier et al., 2008). A detailed comparison of the different targeting techniques for the western North Pacific basin was given in Wu et al. (2009) and for the Atlantic in Majumdar et al. (2006) and Reynolds et al. (2007). One of the popular strategies is to use SVs to identify the "sensitive" regions. In this case, the norm of final-time SVs is confined to the geographical area (verification area) where the forecast must be improved and the initial-time global SVs will indicate the "target area" where extra observations should be taken in order to reduce the forecast error inside the verification area (Buizza and Montani, 1999). Buizza and Montani (1999) suggested to diagnose the "target area" using a localization function based on vertically integrated total energy of SVs ($\boldsymbol{E_j}$) and defined as weighted average of the leading $\boldsymbol{N}$ SVs:

$$f(x) = \frac{1}{N}\sum_{j=1}^{N}\frac{\lambda_j}{\lambda_1}E_j(x). \tag{28}$$

For each case, the target area is defined by the grid points x with the largest $f(x)$. Maps of forecast error variance reduction due to the use of an additional sounding at a given location agree with maps resulting from the former localization function. Buizza and Montani (1999) applied this function to identify "target areas" over the Atlantic in order to reduce the forecast error over Europe; they found that in some cases errors could be reduced by up to 13%.

In more recent papers, Buizza et al. (2007b), Cardinali et al. (2007) and Kelly et al. (2007) investigated the impact of removing targeted observations in the Pacific/Atlantic oceans on the two-day forecast error verified over North America/Europe. They found that observations taken in SV-target areas are more valuable than in randomly selected areas and that the value of targeted observations depends on the region, the season and the baseline observing system (data-rich or data-poor). For example, in a data-poor case, SV-targeted observations over the Pacific reduced the two-day forecasts error of 500-hPa geopotential height in the verification region by 27.5%, while for a data-rich case a reduction of 4.0% was obtained.

For TCs, several studies showed that despite the increased use of satellite data in the analysis of NWP models, additional dropsonde measurements of key variables such as wind, temperature, and humidity below cloud where satellite observing capabilities, are more limited can lead to improvements in track forecasts of the order of 10%–20% (Yamaguchi et al., 2009). Harnisch and Weissmann (2010) investigated the benefit of TORPEX-PARC dropsonde observations in different locations with the ECMWF Integrated Forecasting System (IFS) experiments. As mentioned previously, two regions are often indicated by total-energy SVs as sensitive for a TC: an area in the vicinity of the storm and a remote area associated with a mid-latitude upper trough. Harnisch and Weissmann (2010) found that the largest TC track forecast improvements are found for observations in the vicinity of the storm as indicated by SVs, but only a relatively small influence with a slight positive tendency is observed for dropsondes in remote regions.

Nowadays, in NWP a wide range of satellite observations are used to constrain the analysis (about 95% of the data employed in the 4D-Var system at ECMWF originate from satellites) and this volume of data is increasing. The huge stream of satellite data can be kept to affordable levels if satellite data density is increased only in a selective way

(SV-based thinning). In this context, an important issue is to assess whether SVs can be used to identify areas where extra satellite data can be used to reduce analysis uncertainty and the forecast error (Langland, 2005).

6. Concluding remarks

This article is an introduction to and a review of the singular vectors formulation and properties. Singular vectors (SV) represent the orthogonal set of perturbations that, according to linear theory, will grow fastest over a finite-time interval with respect to a specific metric. Therefore, the study of SVs gives information about the structure and dynamics of rapidly growing perturbations and finite-time instability. SVs are computed for many types of applications in atmospheric science, such as forecast error estimation, ensemble forecasting, target adaptive observations, predictability studies and growth arising from instabilities.

Several choices must be made when SVs are computed: the norms at initial and final time, the optimization time interval (OTI), the trajectory, tangent linear model (TLM) and adjoint model (ADM). The most commonly used norm in various applications is the total-energy norm and the OTI varies usually between 24 hours and 48 hours. The choice of OTI is conditioned by the validity of the tangent linear approximation, which is function of scale. The small scales are dominated by non-linear perturbations growth after 12 hours, while the large scales remain fairly linear out to 48 hours. The resolution of the tangent and adjoint models and OTI change the balance among the contributing mechanism in SV development. Therefore, the choice of parameters must be related to the field of application. For example, an OTI of 48 hours and a dry TLM at a lower horizontal resolution are usually employed for extratropical baroclinic perturbations, while moist perturbations need a moist TLM with higher resolution and an OTI of 24 hours in order to capture the small-scale characteristic of moist processes.

Another important issue in SV computation concerns the number of SVs necessary to capture the growing part of an arbitrary perturbation. While very unstable perturbations evolve usually into the direction of the most unstable SVs, a large number of SVs is needed to describe an arbitrary perturbation. Errico et al. (2001) indicated that the knowledge of most of the spectrum of SVs should be of interest but the computation of a very large number of SVs is not practical because it requires high computational resources.

Nowadays, the attention is focused on the TLM development to include more physical processes in order to approach the TLM to the non-linear model. The linearization of physical processes reveals a lot of difficulties due to the treatment of conditional formulations.

The proper choice of the norm is still an open question, because the key properties of initial-time SVs are strongly norm-dependent. For practical reasons, most studies continue to use the total-energy norm. However, the total-energy initial-time SVs are outside the attractor and, as a consequence, the projection of atmospheric perturbations (or forecast errors) on initial-time SVs is negligible. More efforts are required towards finding an initial-time norm that reveals initial-time SVs similar to atmospheric perturbations.

Most studies that use SVs are in the forecast domain. Only recently SVs have made same inroads in the climate research, where they were employed in analyzing processes with development within a short time window similar to the SV OTI. For example, Diaconescu et al. (2012) use SVs to analyze periods of growth in the internal variability of a Regional Climate Model. Another example is the study of Descamps et al. (2007) that showed that the leading ten SVs couldn't explain mid-latitude cyclogenesis. As a general conclusion, the reader must retain that SVs represent perturbations with a rapid growth over a short period of time, developed into the linear approximation assumption; consequently, they cannot explain non-linear processes that are developing over large periods of time.

Acknowledgments

This manuscript is based upon work supported by the Natural Sciences and Engineering Research Council of Canada (NSERC) Graduate Scholarship (CGSD3), the Canadian Foundation for Climate and Atmospheric Sciences (CFCAS) and the Ouranos Consortium. We thank Dr. Ayrton Zadra for computing the SVs presented in Figs. 1, 2 and 3 and for stimulating discussions during the preparation of this paper. We also thank Prof. Eugenia Kalnay for her comments on a previous version of the paper and Prof. Pierre Gauthier for pointing to us the references of Tanguay et al. and Rabier et al. Comments of the two anonymous reviewers helped in improving the manuscript.

References

Badger, J., Hoskins, B.J., 2001. Simple initial value problems and mechanisms for baroclinic growth. Journal of the Atmospheric Sciences 58, 38–49.
Barkmeijer, J., Buizza, R., Palmer, T.N., 1999. 3D-Var Hessian singular vectors and their potential use in the ECMWF Ensemble Prediction System. The Quarterly Journal of the Royal Meteorological Society 125, 2333–2351.
Barkmeijer, J., Buizza, R., Palmer, T.N., Puri, K., Mahfouf, J., 2001. Tropical singular vectors computed with linearized diabatic physics. The Quarterly Journal of the Royal Meteorological Society 127, 685–708.
Barkmeijer, J., Iversen, T., Palmer, T.N., 2003. Forcing singular vectors and other sensitive model structures. The Quarterly Journal of the Royal Meteorological Society 129, 2401–2423.
Borges, M.D., Hartmann, D.L., 1992. Barotropic instability and optimal perturbations of observed nonzonal flows. Journal of the Atmospheric Sciences 49, 335–353.
Buehner, M., Zadra, A., 2006. Impact of flow-dependent analysis-error covariance norms on extratropical singular vectors. The Quarterly Journal of the Royal Meteorological Society 132, 625–646.
Buizza, R., 1994. Sensitivity of optimal unstable structures. The Quarterly Journal of the Royal Meteorological Society 120, 429–451.
Buizza, R., 1998. Impact of horizontal diffusion on T21, T42, and T63 singular vectors. Journal of the Atmospheric Sciences 55, 1069–1083.
Buizza, R., 2010. The value of a variable resolution approach to numerical weather prediction. Monthly Weather Review 138, 1026–1042.
Buizza, R., Montani, A., 1999. Targeting observations using singular vectors. Journal of the Atmospheric Sciences 56, 2965–2985.
Buizza, R., Palmer, T.N., 1995. The singular-vector structure of the atmospheric global circulation. Journal of the Atmospheric Sciences 52, 1434–1456.
Buizza, R., Tribbia, J., Molteni, F., Palmer, T.N., 1993. Computation of optimal unstable structures for a numerical weather prediction model. Tellus 45A, 388–407.
Buizza, R., Gelaro, R., Molteni, F., Palmer, T.N., 1997. The impact of increased resolution on predictability studies with singular vectors. The Quarterly Journal of the Royal Meteorological Society 123, 1007–1033.
Buizza, R., Bidlot, J.-R., Wedi, N., Fuentes, M., Hamrud, M., Holt, G., Vitart, F., 2007a. The new ECMWF VAREPS. The Quarterly Journal of the Royal Meteorological Society 133, 681–695.
Buizza, R., Cardinali, C., Kelly, G., Thépaut, J.-N., 2007b. The value of observations. II: the value of observations located in singular-vector-based target areas. The Quarterly Journal of the Royal Meteorological Society 133, 1817–1832.
Buizza, R., Leutbecher, M., Isaksen, L., 2008. Potential use of an ensemble of analyses in the ECMWF Ensemble Prediction System. The Quarterly Journal of the Royal Meteorological Society 134, 2051–2066.
Cardinali, C., Buizza, R., Kelly, G., Shapiro, M., Thépaut, J.-N., 2007. The value of observations—Part III: influence of weather regimes on targeting. The Quarterly Journal of the Royal Meteorological Society 133, 1833–1842.
Chen, J.-H., Peng, M.S., Reynolds, C.A., Wu, C.-C., 2009. Interpretation of tropical cyclone forecast sensitivity from the singular vector perspective. Journal of the Atmospheric Sciences 66, 3383–3400.
Cheng, Y., Tang, Y., Zhou, X., Jackson, P., Chen, D., 2010. Further analysis of singular vector and ENSO predictability in the Lamont model—Part I: singular vector and the control factors. Climate Dynamics 35, 807–826.
Coutinho, M.M., Hoskins, B.J., Buizza, R., 2004. The influence of physical processes on extratropical singular vectors. Journal of the Atmospheric Sciences 61, 195–209.
Descamps, L., Ricard, D., Joly, A., Arbogast, P., 2007. Is a real cyclogenesis case explained by generalized linear baroclinic instability? Journal of the Atmospheric Sciences 64, 4287–4308.
Diaconescu, E.P., Laprise, R., Zadra, A., 2012. Singular vector decomposition of the internal variability of the Canadian regional climate model. Climate Dynamics 38, 1093–1113. http://dx.doi.org/10.1007/s00382-011-1179-x.
Ehrendorfer, M., Errico, R.M., 1995. Mesoscale predictability and spectrum of optimal perturbations. Journal of the Atmospheric Sciences 52, 3475–3500.
Ehrendorfer, M., Tribbia, J.J., 1997. Optimal prediction of forecast error covariances through singular vectors. Journal of the Atmospheric Sciences 53, 286–313.
Ehrendorfer, M., Errico, R.M., Raeder, K.D., 1999. Singular vector perturbation growth in a primitive equation model with moist physics. Journal of the Atmospheric Sciences 56, 1627–1648.
Errico, R.M., Raeder, K.D., 1999. An examination of the accuracy of the linearization of a mesoscale model with moist physics. The Quarterly Journal of the Royal Meteorological Society 125, 169–195.

Errico, R.M., Ehrendorfer, M., Raeder, K.D., 2001. The spectra of singular values in a regional model. Tellus 53A, 317–332.
Farrell, B.F., 1982. The initial growth of disturbances in a baroclinic flow. Journal of the Atmospheric Sciences 39, 1663–1686.
Farrell, B.F., 1985. Transient growth of damped baroclinic waves. Journal of the Atmospheric Sciences 42, 2718–2727.
Frederiksen, J.S., 2000. Singular vectors, finite-time normal modes, and error growth during blocking. Journal of the Atmospheric Sciences 57, 312–333.
Gelaro, R., Buizza, R., Palmer, T.N., Klinker, E., 1998. Sensitivity analysis of forecast errors and the construction of optimal perturbations using singular vectors. Journal of the Atmospheric Sciences 55, 1012–1037.
Gilmour, I., Smith, L.A., Buizza, R., 2001. Linear regime duration: is 24 hours a long time in synoptic weather forecasting? Journal of the Atmospheric Sciences 58, 3525–3539.
Hakim, G.J., 2000. Role of nonmodal growth and nonlinearity in cyclogenesis initial-value problems. Journal of the Atmospheric Sciences 57, 2951–2967.
Harnisch, F., Weissmann, M., 2010. Sensitivity of typhoon forecasts to different subsets of targeted dropsonde observations. Monthly Weather Review 138, 2664–2680.
Hartmann, D.L., Buizza, R., Palmer, T.N., 1995. Singular vectors: the effect of spatial scale on linear growth of disturbances. Journal of the Atmospheric Sciences 52, 3885–3894.
Hoskins, B.J., Coutinho, M.M., 2005. Moist singular vectors and the predictability of some high impact European cyclones. The Quarterly Journal of the Royal Meteorological Society 131, 581–601.
Houtekamer, P.L., 1995. The construction of optimal perturbations. Monthly Weather Review 123, 2888–2898.
Isaksen, L., Bonavita, M., Buizza, R., Fisher, M., Haseler, J., Leutbecher, M., Raynaud, L., 2010. Ensemble of data assimilations at ECMWF. Technical Report 636. ECMWF, Shinfield Park, Reading, RG2-9AX, UK, p. 45. Available online at http://www.ecmwf.int/publications/library/do/references/list/14#2010, (accessed 2012.05.01).
Kalnay, E., 2003. Atmospheric modeling, data assimilation and predictability. Cambridge University Press. 341 pp.
Kelly, G., Thépaut, J.N., Buizza, R., Cardinali, C., 2007. The value of observations—Part I: data denial experiments for the Atlantic and the Pacific. The Quarterly Journal of the Royal Meteorological Society 133, 1803–1815.
Kim, H.M., Jung, B.-J., 2009a. Influence of moist physics and norms on singular vectors for a tropical cyclone. Monthly Weather Review 137, 525–543.
Kim, H.M., Jung, B.-J., 2009b. Singular vector structure and evolution of a recurving tropical cyclone. Monthly Weather Review 137, 505–524.
Kleeman, R., Tang, Y., Moore, A.M., 2003. The calculation of climatically relevant singular vectors in the presence of weather noise as applied to the ENSO problem. Journal of the Atmospheric Sciences 60, 2856–2868.
Komori, T., Kadowaki, T., 2010. Resolution dependence of singular vectors computed for typhoon SINLAKU. Scientific Online Letters on the Atmosphere (SOLA) 6, 045–048.
Lacarra, J., Talagrand, O., 1988. Short-range evolution of small perturbations in a barotropic model. Tellus 40A, 81–95.
Langland, R.H., 2005. Issues in targeted observing. The Quarterly Journal of the Royal Meteorological Society 131, 3409–3425.
Leutbecher, M., 2007. On the representation of initial uncertainties with multiple sets of singular vectors optimized for different criteria. The Quarterly Journal of the Royal Meteorological Society 133, 2045–2056.
Leutbecher, M., Palmer, T.N., 2008. Ensemble forecasting. Journal of Computational Physics 227, 3515–3539.
Lorenz, E.N., 1965. A study of the predictability of a 28-variable atmospheric model. Tellus 17, 321–333.
Majumdar, S.J., Aberson, S.D., Bishop, C.H., Buizza, R., Peng, M.S., Reynolds, C.A., 2006. A comparison of adaptive observing guidance for Atlantic tropical cyclones. Monthly Weather Review 134, 2354–2372.
Molteni, F., Palmer, T.N., 1993. Predictability and finite-time instability of the northern winter circulation. The Quarterly Journal of the Royal Meteorological Society 119, 269–298.
Molteni, F., Buizza, R., Palmer, T.N., Petroliagis, T., 1996. The new ECMWF ensemble prediction system: methodology and validation. The Quarterly Journal of the Royal Meteorological Society 122, 73–119.
Montani, A., Thorpe, A.J., 2002. Mechanisms leading to singular-vector growth for FASTEX cyclones. The Quarterly Journal of the Royal Meteorological Society 128, 131–148.
Palmer, T.N., Buizza, R., Molteni, F., Chen, Y.-Q., Corti, S., 1994. Singular vectors and the predictability of weather and climate. Philosophical Transactions of the Royal Society 348, 459–475.
Palmer, T.N., Gelaro, R., Barkmeijer, J., Buizza, R., 1998. Singular vectors, metrics and adaptive observations. Journal of the Atmospheric Sciences 55, 633–653.
Palmer, T.N., Buizza, R., Leutbecher, M., Hagedorn, R., Jung, T., Rodwell, M., Vitart, F., Berner, J., Hagel, E., Lawrence, A., Pappenberger, F., Park, Y.-Y., van Bremen, L., Gilmour, I., Smith, L., 2007. The ECMWF ensemble prediction system: recent and on-going developments. A paper presented at the 36th Session of the ECMWF Scientific Advisory Committee. : ECMWF Research Department Technical Memorandum No. 540. ECMWF, Shinfield Park, Reading, RG2-9AX, UK. Available online at http://www.ecmwf.int/publications/library/do/references/list/14#2010, (accessed 2012.05.01).
Puri, K., Barkmeijer, J., Palmer, T.N., 2001. Ensemble prediction of tropical cyclones using targeted diabatic singular vectors. The Quarterly Journal of the Royal Meteorological Society 127, 709–731.
Rabier, F., Gauthier, P., Cardinali, C., Langland, R., Tsyrulnikov, M., Lorenc, A.C., Gelaro, R., Steinle, P., Koizumi, K., 2008. An update on THORPEX-related research in data assimilation and observing strategies. Nonlinear Processes in Geophysics 15, 1–14.
Reynolds, C.A., Errico, R.M., 1999. Convergence of singular vectors toward Lyapunov vectors. Monthly Weather Review 127, 2309–2323.
Reynolds, C.A., Rosmond, T.E., 2003. Nonlinear growth of singular vector-based perturbations. The Quarterly Journal of the Royal Meteorological Society 129, 3059–3078.
Reynolds, C.A., Peng, M.S., Majumdar, S.J., Aberson, S.D., Bishop, C.H., Buizza, R., 2007. Interpretation of adaptive observing guidance for Atlantic tropical cyclones. Monthly Weather Review 135, 4006–4029.
Reynolds, C.A., Peng, M.S., Chen, J.H., 2009. Recurving tropical cyclones: singular vector sensitivity and downstream impacts. Monthly Weather Review 137, 1320–1337.
Szunyogh, I., Kalnay, E., Toth, Z., 1997. A comparison of Lyapunov and optimal vectors in a low-resolution GCM. Tellus 49A, 200–227.
Tanguay, M., Bartello, P., Gauthier, P., 1995. Four-dimensional data assimilation with a wide range of scales. Tellus 47A, 974–997.
Toth, Z., Kalnay, E., 1997. Ensemble forecasting at NCEP and the breeding method. Monthly Weather Review 125, 3297–3319.
Trevisan, A., Pancotti, F., 1998. Periodic orbits, Lyapunov vectors, and singular vectors in the Lorentz system. Journal of the Atmospheric Sciences 55, 390–398.
Wu, C.-C., Chen, J.-H., Majumdar, S.J., Peng, M.S., Reynolds, C.A., Aberson, S.D., Buizza, R., Yamaguchi, M., Chen, S.-G., Nakazawa, T., Chou, K.-H., 2009. Intercomparison of targeted observation guidance for tropical cyclones in the Northwestern Pacific. Monthly Weather Review 137, 2471–2492.
Yamaguchi, M., Komori, T., 2009. Outline of the typhoon ensemble prediction system at the Japan Meteorological Agency. RSMC Tokyo-Typhoon Center Technical Review, 11, pp. 14–24. Available online at http://www.jma.go.jp/jma/jma-eng/jma-center/rsmc-hp-pub-eg/techrev.htm, (accessed 2011.2.10).
Yamaguchi, M., Iriguchi, T., Nakazawa, T., Wu, C.-C., 2009. An observing system experiment for typhoon Conson (2004) using a singular vector method and DOTSTAR data. Monthly Weather Review 137, 2801–2816.
Zadra, A., Buehner, M., Laroche, S., Mahfouf, J.-F., 2004. Impact of the GEM model simplified physics on extratropical singular vectors. The Quarterly Journal of the Royal Meteorological Society 130, 2541–2569.
Zhang, H., Pu, Z., 2010. Beating the uncertainties: ensemble forecasting and ensemble-based data assimilation in modern numerical weather prediction. Advances in Meteorology. http://dx.doi.org/10.1155/2010/432160 (ID: 432160, 10 pages).